The 10th International Symposium on Flow Visualization
August 26-29, 2002, Kyoto, Japan
F0276

Visualization of Current Vectors in Multi-Layered Printed Circuit Board

Shiraishi, K. *[1], Endo, H. *[1], Hayano, S. *[1], Marinova, I. *[2], and Saito,Y. *[1]

*1 Graduate School of Engineering, Hosei University,
3-7-2 Kajino, Koganei, Tokyo 184-8584, Japan
Tel/ Fax +81-42-387-6200
E-mail:shiraishi@ysaitoh.k.hosei.ac.jp
*2 Department of Electrical Apparatus, Technical University of Sofia, Bulgaria,

Abstract: In order to visualize the current distribution on printed circuit board operating under different frequencies, we have examined the magnetic flux distribution by the strategic dual image method taking open boundary condition into account. Further, we have carried out the experimental verifications to the simulations. We have tried to estimate the current distribution classified into the distinct frequency components by Fourier transform, we have compared with the simulation and experimental data. As a result, fairly good agreement has been obtained.

Keywords: *SDI Method, Visualization, Multi-Layered Printed Circuit Board, Fourier Transform*

1. Introduction

Modern portable electronics are always constructed by thin shape elements such as a printed circuit board (PCB) for carrying as well as handling like one of notebooks. Visualization of the current distributions on the PCB is one of the most reasonable methodologies to inspect their operation and to find their fault parts (Takei et al., 2000). To develop a methodology for current visualization, Miyahara has tried various theoretical and experimental approaches (Miyahara et al., 1998, Sekijima et al, 2000). Also, Shiraishi has applied our methodology to the multi-layered printed circuit boards operating under different frequency (Shiraishi et al, 2001). However, it is difficult to obtain the exact magnetic field exhibiting various electromagnetic actions such as the mutual induction, eddy current and so on.

In order to estimate the open boundary magnetic fields with higher accuracy, we employ a strategic dual image method (SDI), which is based on the essential nature of vector field taking the open boundary effects into account. Employing this approach, we examine the magnetic flux distribution composed of the different frequencies and carry out the experimental verification concerning to the single- and multi-layered PCB models. In this approach, we apply the Fourier transform to the obtained magnetic fields in order to classify them into the distinct frequency components. Further, we try to visualize an each of the current distributions having distinct frequency from those of magnetic fields to both of the simulation and experimental ways. Thus,

we have succeeded in visualizing the current distributions from the magnetic fields taking the mutual actions among the coils in multi-layered PCBs into account.

2. Strategic Dual Image Method

2.1 Governing Equation of Magnetic Field

To represent the quasi-static magnetic field, we utilizes a Helmholtz equation as a governing equation by employing the vector potential $\boldsymbol{A}$.

$$\lambda \nabla^2 \boldsymbol{A} - \kappa \left(\frac{\partial \boldsymbol{A}}{\partial t} \right) = -\sigma \tag{1}$$

where, λ, κ, $\boldsymbol{A}$ and σ denote the reciprocal of permeability, conductivity, magnetic vector potential and current density, respectively. The second term on the left in Eq.(1) represents the time derivative of magnetic flux intensity ,which causes the eddy current density.

2.2 Strategic Dual Image method

The field intensity decreases on moving away from the source point. In addition to this field intensity decrease, the potential may be reduced to zero, so that both the field intensity and potential may reduced to zero at an infinitely long distance from the source point. This means the symmetrical and zero boundary conditions held at the infinitely long distance (Takahashi et al,1993).

At first, let us consider one of the currents i in the problem region under consideration.. When an image current $-(d/a)i$ is imposed at the position shown in Fig.1(a), the normal component of magnetic flux density $\boldsymbol{B}$ becomes zero at the circular/spherical hypothetical boundary. This means that the vector potential $\boldsymbol{A}$ is zero at the hypothetical boundary when the magnetic field is represented in terms of $\boldsymbol{A}$. Moreover, this zero boundary condition $\boldsymbol{A} = 0$ corresponds to the symmetrical boundary condition $\partial \boldsymbol{U} / \partial n = 0$ when the magnetic field is represented in terms of scalar potential $\boldsymbol{U}$. The magnitude of image $-(d/a)i$ depends on the position of field source current i in the hypothetical boundary so that the following condition must be satisfied to reduce the zero net images,

$$a \sum_{p=1}^{q} (i_p / r_p) = 0 , \tag{2}$$

where a is radius of the circle/sphere; r_p ($= a^2/d_p$) is the distance from the center of circle/sphere to the current i_p; and q is the number of current sources. This means that the net currents in the problem region must be zero, and the vector potential $\boldsymbol{A}$ becomes zero at the center of circular/spherical hypothetical boundary.

Secondly, let us consider one of the magnetic charges m in the problem region instead of currents i. When an image $-(d/a)m$ is imposed at the position shown in Fig. 1(b), the tangential component of the field intensity $\boldsymbol{H}$ becomes zero at the hypothetical boundary. This means that the scalar potential $\boldsymbol{U}$ is zero at the hypothetical boundary when the magnetic field is represented in terms of $\boldsymbol{U}$. Moreover, this zero boundary condition $\boldsymbol{U} = 0$ corresponds to the symmetrical boundary condition $\partial \boldsymbol{A} / \partial n = 0$ when the magnetic field is represented in terms of the vector potential $\boldsymbol{A}$. Thus, a combination of the zero and symmetrical boundary solutions leads to an exact open boundary solution even if the finite elements.

2.3 Axisymmetrical open field

As shown in Fig. 2(a), with an arbitrary current *i* flowing toward the ψ direction, this problem can be reduced into an axisymmetrical field problem. When we impose an image current *-i*, as shown in Fig. 2(b), the vector potential A_ψ becomes zero along an ellipse. This means that the hypothetical boundary of axisymmetrical open boundary field becomes an ellipsoid of gyration. Depending on the axial ration *b/a*, a large number of ellipses may be considered so that it is essential to determine a unique axial ratio *b/a* of the ellipsoid as *b/a* = 1.815.
When we introduce this axial ratio *b/a* = 1.815 into the following demagnetization factor formula for an ellipsoid of gyration:

$$N_r = \frac{1}{2[(b/a)^2 - 1]} \times \left[\frac{(b/a)^2}{\sqrt{\{(b/a)^2 - 1\}}} \cos^{-1}\left(\frac{a}{b}\right) - 1 \right], \tag{3}$$

$$N_Z = 1 - 2N_r \tag{4}$$

the demagnetization factors N_Z of the *z* direction and N_r of the *r* direction become N_Z = 0.5 and N_r = 0.25, respectively. This means that this condition makes it possible to calculate the (r, ψ, z) axisymmetrical three-dimensional field problems in the (*r-z*) two-dimensional space(Saito, et al, 1988).

Fig.1 Strategic 2D/3D Dual Images
(a) The rotational field source image –(*d/a*)*i*. The zero $\boldsymbol{A} = 0$ or symmetrical $\partial \boldsymbol{U} / \partial n = 0$ boundary condition is established at the circular/spherical surface.
(b) The divergent field source image –(*d/a*)*m*. The zero $\boldsymbol{U} = 0$ or symmetrical $\partial \boldsymbol{A} / \partial n = 0$ boundary condition is established at the circular/spherical surface.

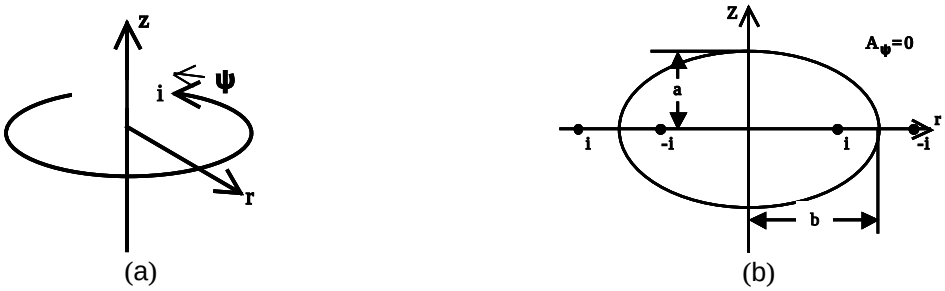

Fig.2 Strategic Dual Image for Axisymmetrical Open Field Problems
(a) An arbitrary current *i* flowing toward the ψ direction
(b) A strategic image current and an elliptical boundary

2.4 Example of SDI Solution along with Finite Elements

Let us consider the problem to obtain the magnetic field from the current flowing on one loop current shown in Fig.3. The current is consisted of only $\theta-$direction component so that the total current in the target region must be zero, thereby; this problem reduces into an axisymmetrical field problem, which can be solved by the SDI method. The governing equation is given by Eq.(5). In Eq.(5), the parameters μ_0, A_θ, J_θ are the permeability of air, magnetic vector potential and current density, respectively.

$$\frac{1}{\mu_0}\nabla^2 A_\theta = -J_\theta \tag{5}$$

Table 1 shows the various constants for the computation. Fig.4 (a) shows the obtained vector potential together with those of analytical one given by Eqs.(6), (7). Fig.4 (b) shows the magnetic flux distribution obtained by curl operation to the vector potential. Thus, it is verified that the SDI method along with finite elements yields a solution well corresponding to those of analytical one.

$$B_\theta(r,z) = \frac{\mu_0 I}{2\pi}\left[\frac{z}{\sqrt{(a+r)^2+z^2}}\right]\left[(\frac{2}{k^2}-1)K(\kappa)-\frac{2}{k^2}K(\kappa)\right](\text{Wb/m}) \tag{6}$$

$$\kappa^2 = \frac{4ra}{(r+a)^2+z^2} \tag{7}$$

Table 1 The Fixed Value for the Calculation

Loop radius a (m)	2
Length of horizontal axes (m)	3
Length of vertical axes(m)	3×1.815
Permeability(vacuum) μ_0 (H/m)	$4\pi\times10^{-7}$
Current I (A)	1

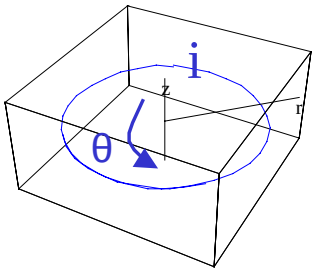

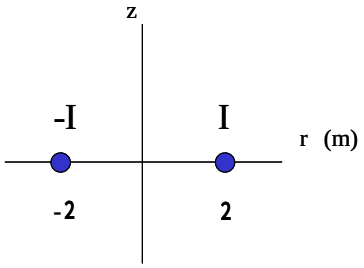

Fig. 3 Example of Loop Current

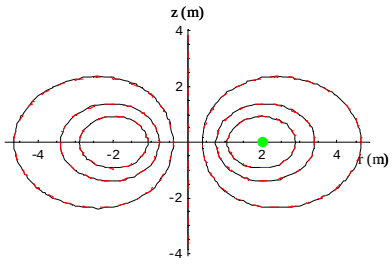

(a)

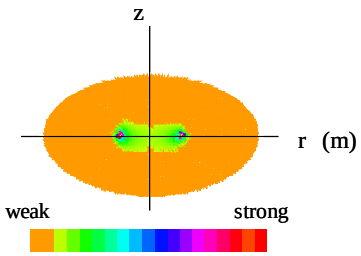

(b)

Fig.4 Result of Example Problem
(a) Dashed line: SDI Solid line: Analytical
(b) The Magnetic flux distribution

3. Simulations and Experiment

3.1 PCB Models

Fig.5 shows the two PCB models. We compute the time domain magnetic flux generated by the 11 by 11 cm² current flowing surface. One is the single-layered model [Ⅰ], and the other is the three-layered model [Ⅱ]. The measurement surfaces are set to the parallel surface above the target surface to the model [Ⅰ], and also both of the top and bottom surface to the model [Ⅱ] as shown in Fig.5. The measurement interval is 1cm. Table 1 shows the various constants of the models. The parameters in Eq.(1) μ, κ are set to $4\pi\times10^{-7}$ (H/m) and 5.8×10^{7} (S/m), respectively.

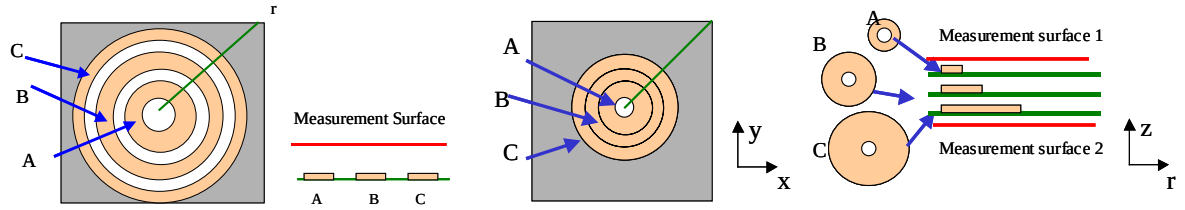

[Ⅰ] Single-layered model [Ⅱ] Multi-layered model

Fig. 5 PCB Models

Table 2 Various Constants of the PCB Models

Model [Ⅰ]

	Coil A	Coil B	Coil C
Wire of diameter (mm)	0.8	0.8	0.8
Turn	10	10	10
Internal diameter (mm)	5	20	35
External diameter (mm)	13	27	43
Exciting amplitude (A)	0.2	0.2	0.2
Frequency (kHz)	10	30	50
Distance from measured surface (mm)	6	6	6

Model [Ⅱ]

	Coil A	Coil B	Coil C
Wire of diameter (mm)	0.8	0.8	0.8
Turn	10	20	30
Internal diameter (mm)	5	5	5
External diameter (mm)	13	21	29
Exciting amplitude (A)	0.3	0.3	0.3
Frequency(kHz)	10	30	50
Distance from measured surface top/bottom (mm)	6 / 13	9 /10	13 / 6

3.2 Experimental Verification

To verify the validity of our simulation, we have carried out the experiment to the PCB models. Fig.6 shows the tested current carrying coils. We have measured the waveforms of the output voltage induced in the search coils located at the top and bottom parallel surfaces. The number of measured points is the 11 by 11 points.

According to Faraday's Law, a relationship between the conduction voltage v(t) and magnetic flux $\varphi(t)$ is given by.

$$v(t) = -N\frac{d\varphi(t)}{dt} \tag{8}$$

N in Eq.(8) is the number of turns of the search coil. Therefore, the linkage magnetic flux is obtained by the time integral operation to the induced voltage v(t) in Eq.(8). Measured induced voltage v(t) to the multi-layered coils operating under different frequencies is shown in Fig.7. Under the assumption that non-linear material is not contained, it is possible to apply the Fourier

transform. This transform classifies the voltage v(t) into the distinct time frequency components. Fig.8 shows the Fourier spectram of the measured induced voltage v(t). In Fig.8, the upper and lower Fourier spectra are the entire and lower frequencies components. Apply the inverse Fourier transforms to each of the lower frequency components yield the frequency-classified original waveforms. The uppers in Figs.9-10 show the frequency-classified contour lines. The white, gray and black parts in these contour lines refer to the high, low and zero magnitudes, respectively. The lowers in Figs.9-10 show the peak values at the 11 by 11-measured points.

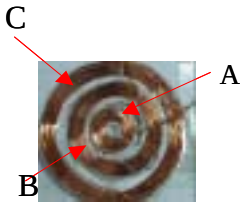

Model [Ⅰ]

Model [Ⅱ]

Fig.6 Tested Exiting Coils

.

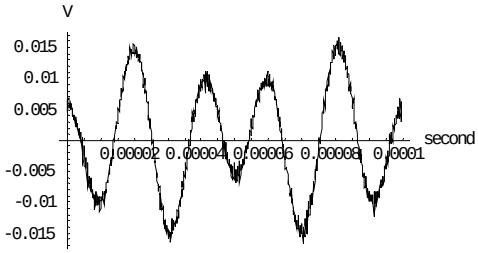

Fig.7 Measured Waveform

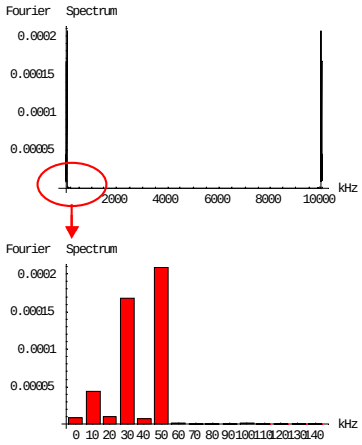

Fig.8 Fourier Spectrum

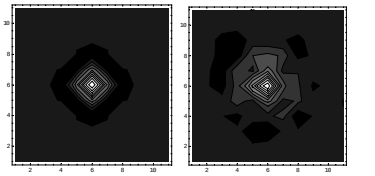

Left: SDI solution, Right: Experimented

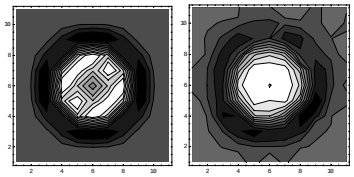

Left: SDI solution, Right: Experimented

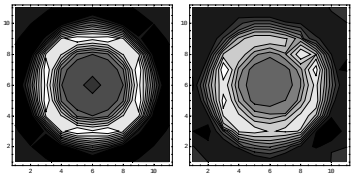

Left: SDI solution, Right: Experimented

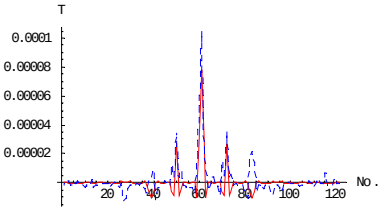

10(kHz)

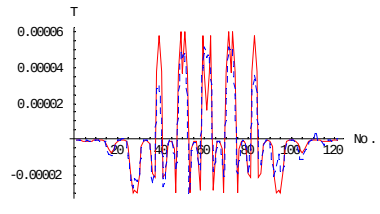

30(kHz)

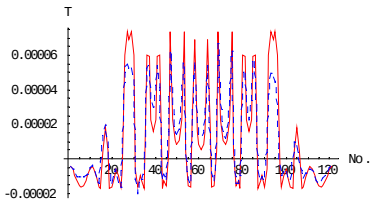

50(kHz)

Fig.9 Frequency-Classified Components (Model [Ⅰ])
Solid line: SDI solution Dotted line: Experimented

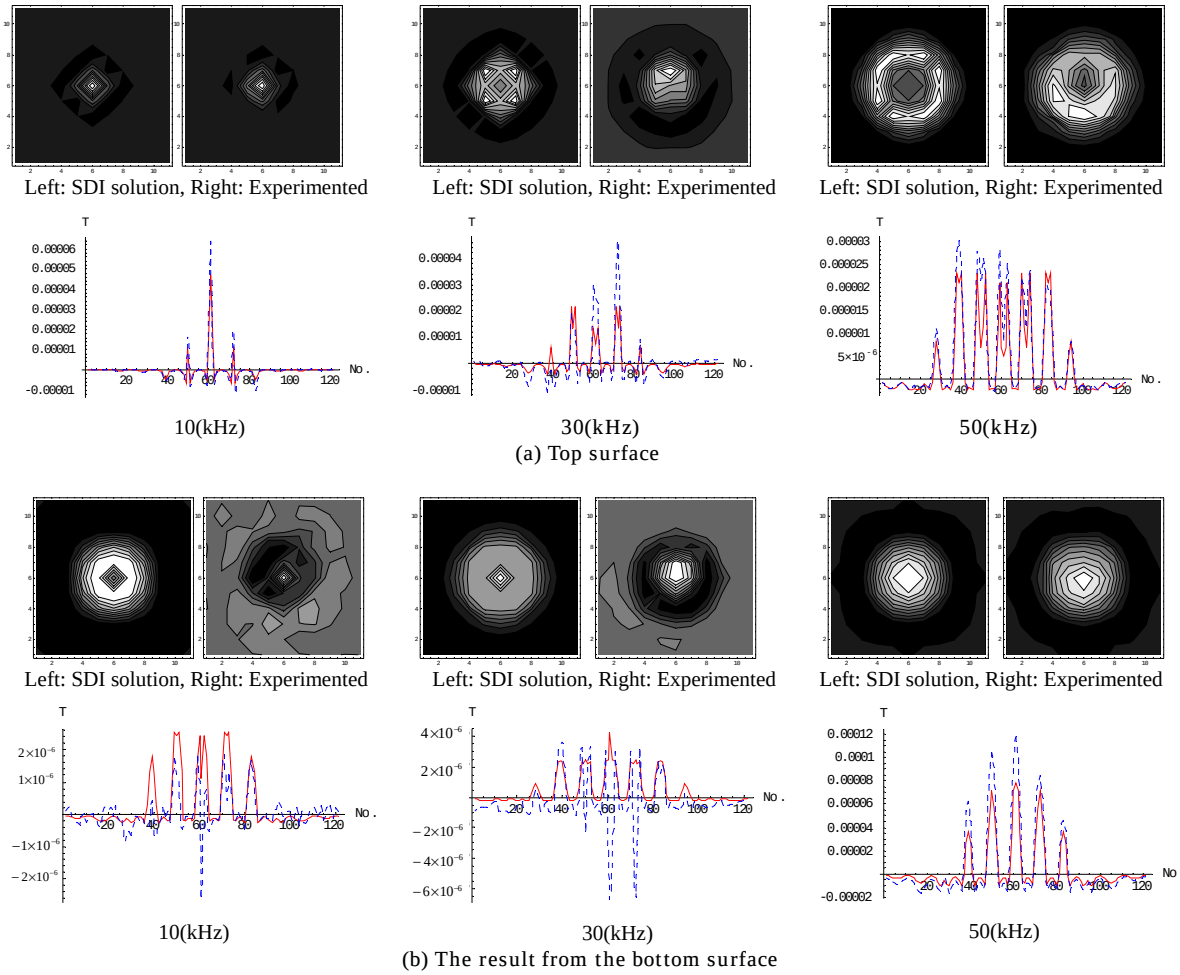

Fig.10 Frequency-Classified Components (Model [Ⅱ])
Solid line: SDI solution Dotted line: Experimented

4. Visualization of Current Distribution

4.1 Loop Current Model

Let us consider the problem to visualize the current distribution by measuring the local magnetic fields. As is well known, a relationship between the magnetic flux density B and the magnetic field H is given with the permeability μ,

$$B = \mu H \tag{9}$$

Fig.11 shows a typical example of a loop current i and magnetic field H. As shown in Fig.12, let us assume that the current flowing surface is divided into a large number of the loop currents. A relationship between the loop current and magnetic field is given in terms of the elliptic integrals $E(\kappa), K(\kappa)$ as

$$H_z = \frac{1}{2\pi}\left[\frac{z}{\sqrt{(a+r)^2+z^2}}\right]\left[\frac{a^2-r^2-z^2}{(a-r)^2+z^2}E(\kappa)+K(\kappa)\right] \tag{10}$$

where the parameters a, r, z are shown in Fig.11 and also, κ is given by Eq.(7). By means of this model, it is possible to derive a following system of equation:

$$\boldsymbol{Y} = C\boldsymbol{X} \tag{11}$$

where **Y**, **X** are the vectors with values of the measured magnetic fields and loop currents with order *n*, respectively. *C* is a n^{th} order square system matrix, which is derived along with the elliptic integral functions. If it is possible to obtain an inverse matrix of *C*, then the loop currents vector **X** can be evaluated. Applying curl operation to the vector **X** yields the current vector distribution on the PCBs.

4.2 Current Visualization

Figs.13 -14 show the current vector distributions estimated from the results in Figs.9-10 along with the system matrix derived by Eq.(10). By observing the results in Fig.13, the dominant current vectors suggest the shape of the coils excited by the distinct frequency. Further, it is possible to observe the effect of mutual induction among the coils in the results of 30(kHz) and 50(kHz). By considering the results in Fig.14, it is obvious that the effect of mutual induction is more intensive compared with those of Fig.13. This means that the mutual induction among the multi-layered PCBs dominates the magnetic field distribution around the target PCBs.

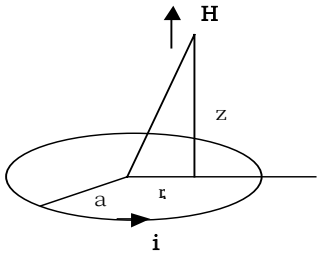

Fig.11 Relationship Between the Loop Current **i** and Magnetic Field **H**.

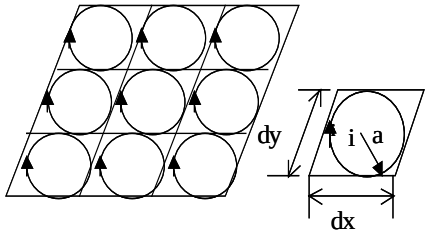

Fig.12 Subdivided Loop Currents Model.

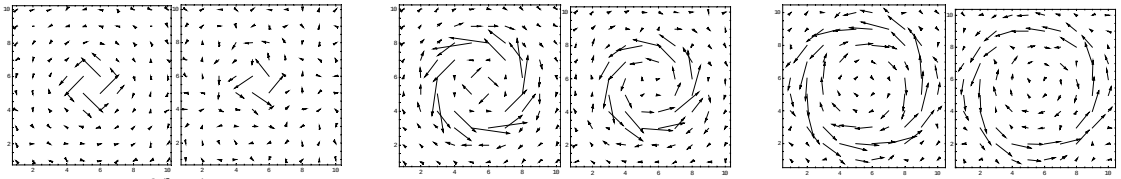

10(kHz) 30(kHz) 50(kHz)
Left: SDI solution, Right: Experimented

Fig.13 Visualized Current Distributions (Model Ⅰ)

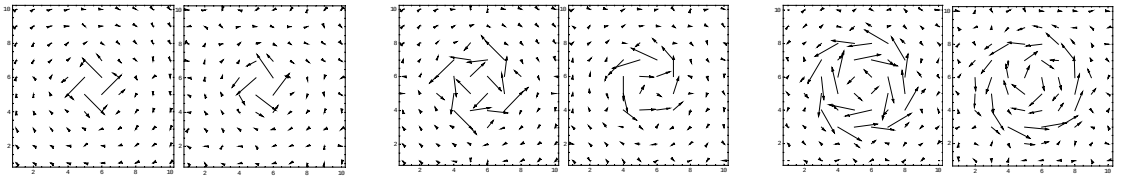

10(kHz) 30(kHz) 50(kHz)
Left: SDI solution, Right: Experimented

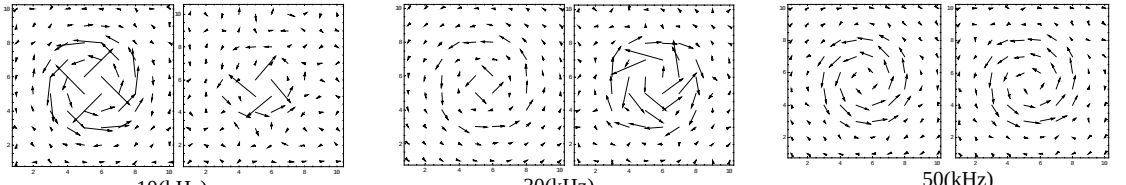

10(kHz) 30(kHz) 50(kHz)
Left: SDI solution, Right: Experimented

Fig.14 Visualized Current Distributions (Model Ⅱ)

5. Conclusion

In order to estimate the open boundary magnetic fields with higher accuracy, we have employed the strategic dual image method, which is based on the essential nature of vector field taking the open boundary effects into account. Employing this approach, we have examined the magnetic flux distribution composed of the different frequencies and carried out the experimental verification concerning to the single-layered and multi-layered PCB models. In this approach, we have applied the Fourier transform to the obtained magnetic fields in order to classify them into the distinct frequency components. Further, we have tried to visualize an each of the current distributions having distinct frequency from those of magnetic fields to both of the simulation and the experimental ways. Thus, we have succeeded in visualizing the current distributions from the magnetic fields taking the mutual actions among the coils in multi-layered PCBs into account.

References

Takei,A., Hayano,S., and Saito,Y., 2000, “A Weighed Inverse Matrix Approach to Searching for the Electric Field Sources,” *IEEE Trans. Magn.*, Vol. 36, No. 4, pp1031-1034.

Miyahara,S., Hayano,S., Toya,T., and Saito,Y., 1998, ”Visualization of electromagnetic fields distribution near the electric and electronic devices—Principle and initial experiments—,” *Paper on Technical meeting of Magnetics Society of IEEJ,* MAG-98-112.

Sekijima,D., Miyahara,S., Hayano,S., and Saito,Y., 2000, ”A study of Visualization of Quasi-3Dimensional Current Distribution”, *IEE Japan Trans,* Vol.120-A, No.10, pp.907-912.

Shiraihi,K., Hayano,S., and Saito,Y., 2001, “A Method of Frequency Classified Currents Estimation on Multi-Layered Circuit Board”, *The Magnetics Society of IEE of Japan* , MAG-01-214 (In Japanese)

Takahashi,K, Hayano,S. and Saito, Y., 1993, “The Strategic Dual Image Method for the Open Boundary Electromagnetic Field Problem”, *International Journal of the Applied Electromagnetic in Materials,* Vol.4 , E0003-A pp179-184..

Saito,Y. Takahashi,K. and Hayano,S. 1988 ,“ Finite element solution of unbounded magnetic field problem containing ferromagnetic materials “ *, IEEE Transaction on Magnetics*, Vol.MAG-24, No.6.